

## PROBING THE $Z > 6$ UNIVERSE WITH THE FIRST HUBBLE FRONTIER FIELDS CLUSTER ABELL 2744 <sup>†</sup>

HAKIM ATEK<sup>1</sup>, JOHAN RICHARD<sup>2</sup>, JEAN-PAUL KNEIB<sup>1,3</sup>, BENJAMIN CLEMENT<sup>4</sup>, EIICHI EGAMI<sup>4</sup>, HARALD EBELING<sup>5</sup>,  
MATHILDE JAUZAC<sup>6</sup>, ERIC JULLO<sup>3</sup>, NICOLAS LAPORTE<sup>7,8</sup>, MARCEAU LIMOUSIN<sup>3</sup>, AND PRIYAMVADA NATARAJAN<sup>9</sup>

*Draft version September 11, 2018*

### ABSTRACT

The Hubble Frontier Fields (HFF) program combines the capabilities of the *Hubble Space Telescope* (*HST*) with the gravitational lensing of massive galaxy clusters to probe the distant Universe to an unprecedented depth. Here, we present the results of the first combined *HST* and *Spitzer* observations of the cluster Abell-2744. We combine the newly acquired near-infrared data with ancillary optical images to search for gravitationally lensed high-redshift ( $z \gtrsim 6$ ) galaxies. We report the detection of 17  $I_{814}$ -dropout candidates and one  $Y_{105}$ -dropout in a total survey area of 1.43 arcmin<sup>2</sup> in the source plane. The predictions of our lens model allow us to also identify five multiply-imaged systems lying at redshifts between  $z \sim 6$  and  $z \sim 8$ . Thanks to constraints from the mass distribution in the cluster, we were able to estimate the effective survey volume corrected for completeness and magnification effects. This was in turn used to estimate the rest-frame ultraviolet luminosity function (LF) at  $z \sim 6 - 8$ . Our LF results are generally in agreement with the most recent blank field estimates, confirming the feasibility of surveys through lensing clusters. Although based on shallower observations than what will be achieved in the final dataset including the full ACS observations, the LF presented here extends down to  $0.2L^*$  at  $z \sim 7$  thanks to the highly-magnified survey areas. This early study forecasts the power of using massive galaxy clusters as cosmic telescopes and its complementarity to blank fields.

*Subject headings:* gravitational lensing: strong, galaxies: high-redshift, galaxies:surveys

### 1. INTRODUCTION

The discovery of the first galaxies to assemble in the Universe has long been one of the most exciting challenges of observational cosmology. The identification of these high-redshift sources in deep blank fields relies mostly on the photometric detection of the IGM absorption blueward  $\text{Ly}\alpha$ , or the Lyman break technique (Steidel et al. 1996; Giavalisco et al. 2004). Great progress has been made in characterizing the early galaxy population at  $z \sim 6 - 7$  through the determination of their UV colors, stellar masses or ages (McLure et al.

2011; Bouwens et al. 2012; Richard et al. 2011) owing to unprecedented capabilities of the Wide Field Camera 3 (WFC3) onboard *HST*. Far from the several thousands of galaxies confirmed up to a redshift of 6.5, we are starting to spectroscopically confirm few galaxies at  $z > 7$  (Vanzella et al. 2011; Schenker et al. 2012; Ono et al. 2012; Finkelstein et al. 2013). The decrease of the prevalence of  $\text{Ly}\alpha$  emitters at  $z > 7$  might be a direct indication of the increase in the opacity of the intergalactic medium (IGM), which greatly attenuates the  $\text{Ly}\alpha$  line through resonant scattering (e.g., Stark et al. 2010). Recent studies also suggest that the  $\text{Ly}\alpha$  luminosity function decreases at  $z > 7$  indicating an increase in the neutral gas fraction in the intergalactic medium (IGM, Kashikawa et al. 2006; Ouchi et al. 2010). However, such conclusions are still prone to large uncertainties because of the small sample size, as near-infrared (NIR) observations of faint sources at  $z > 7$  is extremely challenging. Of course, one key driver for these studies of early galaxies is to determine the sources responsible for re-ionization of the high redshift Universe.

A complementary approach is to exploit gravitational lensing offered by massive galaxy clusters (Kneib & Natarajan 2011), which magnifies the brightness of intrinsically faint sources. This has been successfully used to detect galaxies over a wide redshift range, taking advantage of the flux magnification (e.g. Kneib et al. 2004; Bouwens et al. 2009; Richard et al. 2011; Alavi et al. 2013) and the higher spatial resolution for detailed, small-scale studies of high-redshift galaxies (e.g., Brammer et al. 2012). Combining the exquisite capabilities of *HST* with the power of “gravitational telescopes”, the new *HST* Frontier Fields<sup>11</sup> (HFF) initiative is aiming to peer deeper into the distant Universe by

<sup>†</sup> Based on observations made with the NASA/ESA Hubble Space Telescope, which is operated by the Association of Universities for Research in Astronomy, Inc., under NASA contract NAS 5-26555. These observations are associated with programs 13495 and 11689. Based in part on observations made with the Spitzer Space Telescope, which is operated by the Jet Propulsion Laboratory, California Institute of Technology under a contract with NASA.

<sup>1</sup> Laboratoire d’Astrophysique, Ecole Polytechnique Fédérale de Lausanne, Observatoire de Sauvigny, CH-1290 Versoix, Switzerland

<sup>2</sup> CRAL, Observatoire de Lyon, Université Lyon 1, 9 Avenue Ch. André, 69561 Saint Genis Laval Cedex, France

<sup>3</sup> Aix Marseille Université, CNRS, LAM (Laboratoire d’Astrophysique de Marseille) UMR 7326, 13388, Marseille, France

<sup>4</sup> Steward Observatory, University of Arizona, 933 North Cherry Avenue, Tucson, AZ, 85721, USA

<sup>5</sup> Institute for Astronomy, University of Hawaii, 2680 Woodlawn Drive, Honolulu, Hawaii 96822, USA

<sup>6</sup> Astrophysics and Cosmology Research Unit, School of Mathematical Sciences, University of KwaZulu-Natal, Durban, 4041 South Africa

<sup>7</sup> Instituto de Astrofísica de Canarias (IAC), E-38200 La Laguna, Tenerife, Spain

<sup>8</sup> Departamento de Astrofísica, Universidad de La Laguna (ULL), E-38205 La Laguna, Tenerife, Spain

<sup>9</sup> Department of Astronomy, Yale University, 260 Whitney Avenue, New Haven, CT 06511, USA

<sup>11</sup> <http://www.stsci.edu/hst/campaigns/frontier-fields/>

initially devoting a total of 560 orbits to observe four clusters down to magnitude limit of  $\sim 29$ . Over Cycles 21 and 22, the program will obtain deep optical and NIR imaging in seven filters using ACS and WFC3 for both the clusters and the parallel blank fields.

Here we present the first results of the NIR observations of the Abell-2744, where we search for high-redshift candidates at  $z \sim 6 - 8$  behind the galaxy cluster. In Section 2, we present the observational dataset and reduction steps leading to the construction of the source catalog. The procedure used to select high-redshift candidates is detailed in Section 3 together with the sources of contamination. In Section 4 we present the luminosity distribution at  $z \sim 6 - 8$  and compare to previous blank field results. We use a standard  $\Lambda$ CDM cosmology with  $H_0 = 71 \text{ km s}^{-1} \text{ Mpc}^{-1}$ ,  $\Omega_\Lambda = 0.73$ , and  $\Omega_m = 0.27$ . Magnitudes are in AB system.

## 2. OBSERVATIONS AND DATA REDUCTION

In this paper we combine existing imaging and spectroscopic data obtained in previous *HST* campaigns targeting A2477 cluster with new *HST* IR observations that were taken as part of the Frontier Fields program. The resulting pseudo-color image is shown in Figure 2.

### 2.1. Previous HST Data

Optical observations were obtained with the Advanced Camera for Survey (ACS) onboard *HST* in cycle 17 (GO 11689, PI: Dupke) and used in the strong lensing analysis presented in Merten et al. (2011). Images were taken with the Wide Field Camera (WFC) using three broadband filters F435W, F606W, and F814W. A summary of the dataset is presented in Table 1. For the basic reduction steps, we used the CALACS package v2012.2 that include Charge Transfer Efficiency (CTE) corrections, which were not available in the publicly-released reductions. Then all exposures in each filter were median combined using *Astrodrizzle* task in the new STSDAS/Drizzlepac package<sup>12</sup>. First, the different exposures were corrected for small misalignments using *Tweakreg* before rejection of cosmic rays and correction for geometrical distortions. The final images have a pixel scale of  $0.05'' \text{ pix}^{-1}$  and reach a  $5-\sigma$  depth (for point sources in  $0.4''$  aperture) of 27.6, 27.5, and 27.4 in F435W, F606W, and F814W, respectively.

### 2.2. Hubble Frontier Fields Data

The NIR observations of the first cluster in the HFF program (GO/DD 13495), using the Wide Field Camera 3 (WFC3), started on October 25th 2013. This includes imaging in four filters F105W, F125W, F140W, F160W, that will ultimately achieve a total exposure time of 24, 12, 10, and 24 orbits, respectively. Here we use the first four epochs of observations summarized in Table 1. Basic reductions were once again performed using *HSTCAL* and most recent calibration files. Individual frames were coadded using *Astrodrizzle* after registration to the ACS reference image using *Tweakreg* shift file. After an iterative process, we achieve an alignment accuracy of 0.1 pixel between WFC3 and ACS images. The final images have  $0.13''$  pixel size and a  $5-\sigma$  depth reached

TABLE 1  
SUMMARY OF *HST* OBSERVATIONS

Target	R.A. (J2000)	Dec	Instrument/Filter	$t_{\text{obs}}$
A-2744	00 14 21.3	-30 23 48	WFC3/F160W	46570
A-2744	00 14 21.3	-30 23 48	WFC3/F140W	22432
A-2744	00 14 21.3	-30 23 48	WFC3/F125W	16324
A-2744	00 14 21.3	-30 23 48	WFC3/F105W	46520
A2744-S	00 14 18.6	-30 23 37	ACS/F814W	13248
A2744-S	00 14 18.6	-30 23 37	ACS/F606W	13250
A2744-S	00 14 18.7	-30 23 34	ACS/F435W	16162

in the NIR filters is 28.5 (F105W), 28.3 (F125W), 28.4 (F140W), and 28.5 (F160W) respectively.

### 2.3. Spitzer Data

*Spitzer* imaging of Abell 2744 using Infrared Array Camera (IRAC) was obtained on September 2013 as part of the Frontier Field *Spitzer* program (PI : T. Soifer). The dataset we used here represents 50% of the planned observations for the cluster. The total exposure time is 25 hours on sources in each of the 2 IRAC channels 3.6 and 4.5 microns. We used corrected Basic Calibrated Data (cBCD) images, that are provided by the *Spitzer* Science Center and automatically corrected by pipeline for various artifacts (such as muxbleed, muxstripe, and pulldown). The cBCD frames and associated mask and uncertainty images were processed, drizzled and combined into final mosaics using the standard SSC reduction software MOPEX. The mosaic has a  $2-\sigma$  point source sensitivity (measured from the noise in a clean area) of 0.093 and  $0.148 \mu\text{Jy}$  in the 3.6 and 4.5 micron channel respectively.

### 2.4. Photometric Catalogs

We used a deep (F125W+F140W) image for source detection with SExtractor software (Bertin & Arnouts 1996). First, all images were PSF-matched to the F160W image with a PSF model derived using *Tiny Tim* (Krist et al. 2011). Then we ran SExtractor in dual mode with the deep IR image as detection frame and the image in each filter to perform the photometry within the same aperture. The isophotal magnitude is adopted for the color determination and a local background calculation is adopted for the photometry. The final drizzling was performed with the inverse variance map to account for all the sources of uncertainties in the image. Then this weight map was transformed to an *rms* map including the correlated noise correction (Casertano et al. 2000) to derive flux uncertainties during source extraction.

## 3. CANDIDATE SELECTION

For the selection of high-redshift candidates, we adopted the commonly used dropout criteria based on the Lyman break technique (Steidel et al. 1996; Giavalisco et al. 2004). For  $I_{814}$  dropouts we adopted the following criteria (see for example Oesch et al. 2010):

$$\begin{aligned}
 (I_{814} - Y_{105}) &> 0.8 \\
 (I_{814} - Y_{105}) &> 0.6 + 2(Y_{105} - J_{125}) \\
 (Y_{105} - J_{125}) &< 0.8
 \end{aligned} \tag{1}$$

<sup>12</sup> <http://drizzlepac.stsci.edu>

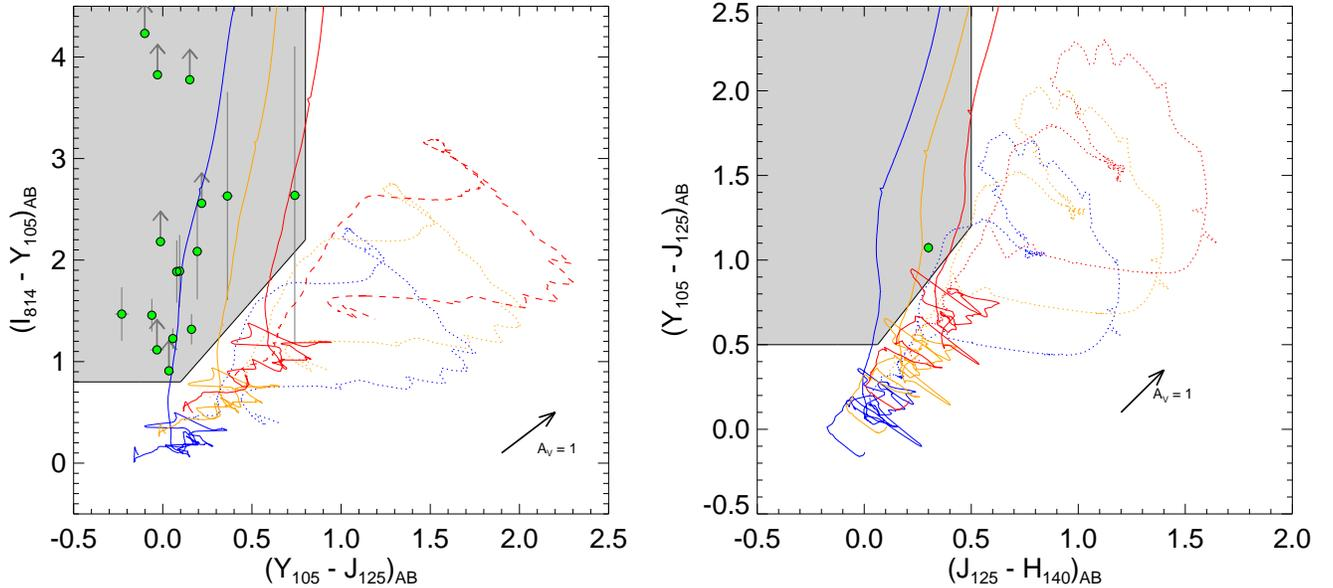


FIG. 1.— Color-Color selection of  $z \sim 6-7$  (left panel) and  $z \sim 8$  (right panel) candidates. The dropout candidates are represented by green circles with  $1-\sigma$  uncertainties and the selection window by the shaded region. We also show the expected color tracks as a function of redshift for starburst galaxies (solid lines) and elliptical galaxies (dotted lines). The color code indicates an increase of attenuation from  $A_V = 0$  (in blue) to  $A_V = 2$  (in red). We used standard galaxy templates from of Coleman et al. (1980) and Kinney et al. (1996).

In order to more efficiently reject low- $z$  interlopers the second criterion is more stringent than what has been used previously to identify similar sources (see Fig. 1). We also require that the candidates are detected in  $Y_{105}$  and  $J_{125}$  bands with a minimum of  $5-\sigma$  significance while they remain undetected in the optical  $B_{435}$  and  $V_{606}$  bands at less than  $2-\sigma$ . Objects that are not detected in the  $I_{814}$  filter are assigned a  $3-\sigma$  lower limit for their continuum break. To identify the  $Y_{105}$  dropouts we applied the following color selection:

$$\begin{aligned} (Y_{105} - J_{125}) &> 0.5 \\ (Y_{105} - J_{125}) &> 0.4 + 1.6(J_{125} - H_{140}) \\ (J_{125} - H_{140}) &< 0.5 \end{aligned} \quad (2)$$

Similarly, we require a  $5\sigma$  detection in the bands redward of the break and no detection in all the bands blueward the break. The selection procedure is illustrated in Fig. 1, where the left and right panels show the  $z \sim 6-7$  and  $z \sim 8$  selections, respectively. Objects satisfying our dropout selection (shaded box) are represented by green circles with  $1-\sigma$  uncertainties. We also plot the color tracks of different galaxy types as a function of redshift and for three values of attenuation. We used standard libraries of Coleman et al. (1980) to calculate the tracks of elliptical galaxies (dotted lines) and Kinney et al. (1996) for star-forming galaxies (solid lines). The blue, orange and red colors represent an attenuation of  $A_V=0, 1$ , and  $2$ , respectively. All objects are visually inspected to remove spurious detections or contaminated photometry from close objects. Our final sample consists of 17 candidates at  $z \sim 7$  and one candidate at  $z \sim 8$ . The  $Y_{105}$ -dropout is shows a flux excess in the  $4.5 \mu\text{m}$  IRAC band while it is undetected in the  $3.5 \mu\text{m}$  channel. This is possibly due to the contribution of the redshifted [OIII] +

$\text{H}\beta$  emission lines. A detailed analysis of the properties of this candidate and discussion of its high-redshift solution will be presented in Laporte et al. (2013). Because the optical ACS data do not match the depth of the new IR observations, we restricted the search to relatively bright candidates. The identification of fainter objects will be possible with future deep ACS observations of the same HFF program.

### 3.1. Contamination

Possible sources of contamination include low-redshift galaxies that enter the selection space. This can occur when strong nebular emission lines contribute to the total flux in one filter, mimicking a continuum break (Atek et al. 2011). However, the use of multiple and contiguous filters greatly mitigates the contamination from such sources, since the emission line should be isolated and the flux enhancement restricted to only one filter (or two in the case of a combination of lines such as  $\text{H}\alpha$  and [OIII]). Low- $z$  interlopers with unusually high reddening or extremely old stellar population, although rare, could also be selected mistakenly as high- $z$  dropouts (Hayes et al. 2012). The colors of most of our candidates suggest a rather blue continuum incompatible with the existence of such a red population. Finally, cool dwarf stars occupy a close but separate region in color-color space from our selection window and can be identified as point-like sources from their light profiles or the stellarity parameter of SExtractor (i.e. stellarity  $> 0.6$ ).

### 3.2. Photometric Redshifts

Additionally, we computed photometric redshifts for our candidates by fitting the photometric data with spectral energy distribution (SED) templates using the Hyperz software (Bolzonella et al. 2000). We used standard

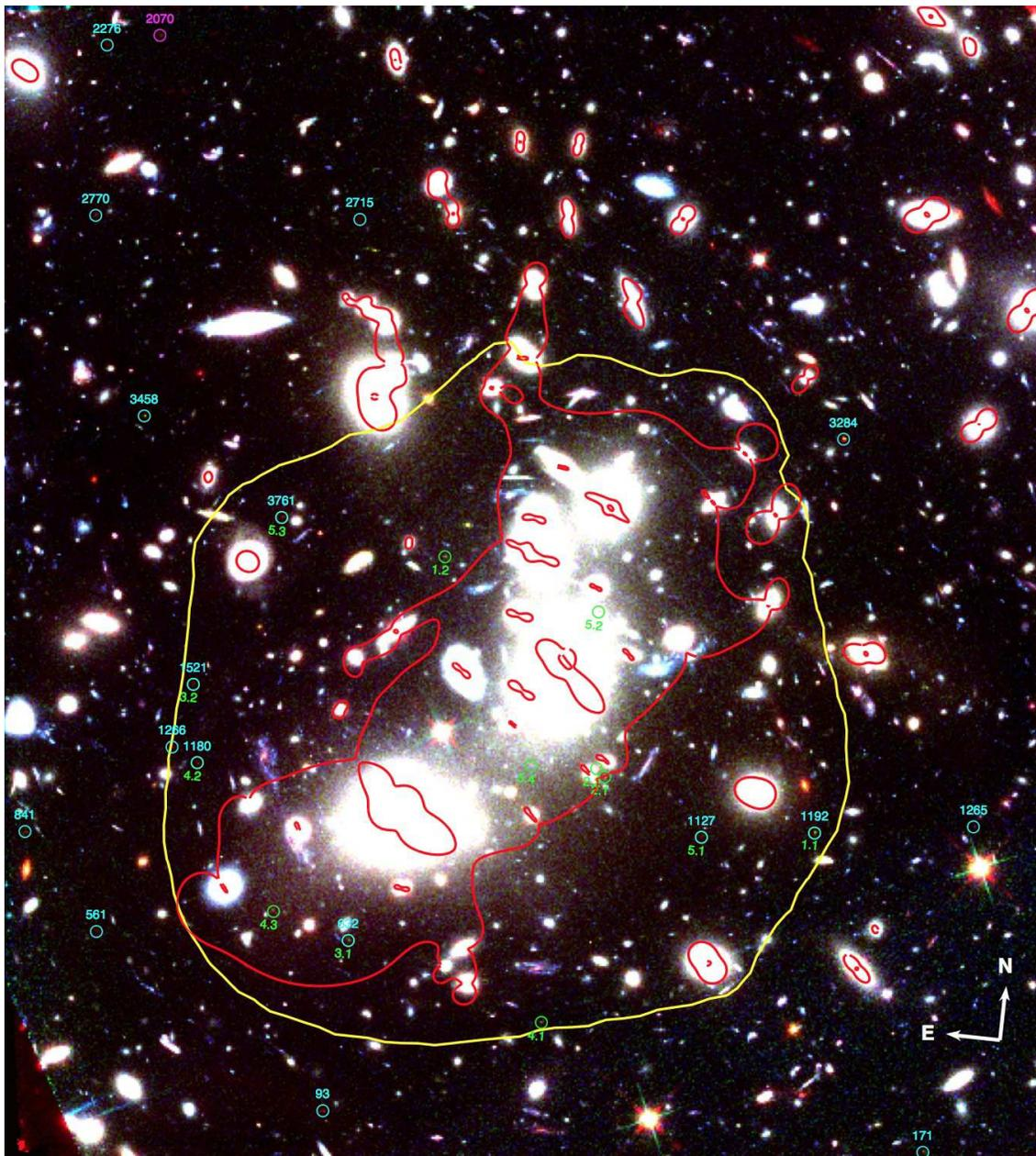


FIG. 2.— The location of the drop-out images is superposed on the strong lensing model for Abell 2744 (Richard et al., in prep). The pseudo-color image is a combination of the F606W, F814W and a deep (four IR bands stack) WFC3/IR image. Overlaid in red are the critical lines for background sources at  $z = 7$ . The position of the candidates at  $z = 6 - 7$  and  $z \sim 8$  are marked with cyan and magenta circles, respectively. The green circles show the positions of the multiple-image systems identified with the predictions from the mass model, while the yellow line is the predicted region for multiple images.

stellar population libraries of Bruzual & Charlot (2003) and a Salpeter (1955) initial mass function (IMF). We find that the probability distribution of the photometric redshifts all indicate a high- $z$  solution in agreement with the color-color selection. The photometric and color information of the candidates are presented in Table 2. We also include in the same table the best-fit redshift given by the probability distribution function for each galaxy, together with the magnification factors. Figures 3 and 4 show the image cutouts of the  $z \sim 6 - 7$  and 8 candidates in the ACS, WFC3, and IRAC filters.

### 3.3. Multiple Images

Strong lensing creates multiple images of the same background galaxy, whose locations can be predicted by our lens model (Richard et al., in prep). For each object selected by our color-color selection, we visually search the field for additional counter-images according to their photometric redshift, color and position. We also looked for multiply-imaged systems that did not satisfy our selection criteria, mainly because of their low signal to noise ratio. We identified two double-images, two triple-images, and one quadruple-image system between  $6 \lesssim z \lesssim 8$ , which are presented in Table 3 and Fig-

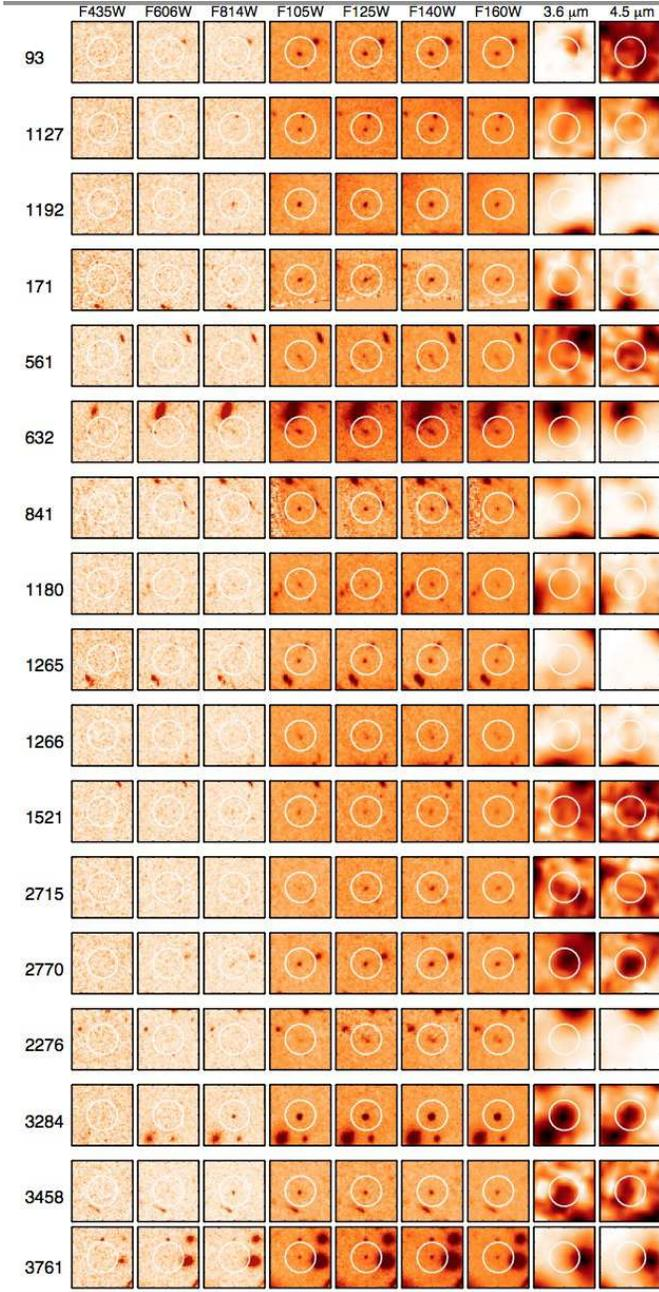


FIG. 3.— Postage stamps of the  $z \sim 6-7$  candidates in the ACS  $F_{435W}$ ,  $F_{606W}$ ,  $F_{814W}$ , WFC3  $F_{105W}$ ,  $F_{125W}$ ,  $F_{140W}$ ,  $F_{160W}$  and IRAC  $3.6 \mu m$ ,  $4.5 \mu m$  bands. The size of each cutout is about  $5''$  and the white circle denotes the source position. Sources show a strong  $J_{814} - J_{105}$  and remain undetected at a  $2 - \sigma$  level in the  $B_{435}$  and  $V_{606}$  bands.

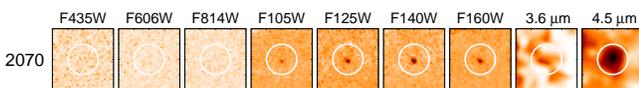


FIG. 4.— same as Fig. 3 for a  $z \sim 8$  candidate. The source has a strong  $J_{105} - J_{125}$  break with no detection at a  $2 - \sigma$  level in the  $B_{435}$ ,  $V_{606}$ , and  $I_{814}$  bands. It is detected in all WFC3 filters redward the break with at a minimum of  $5 - \sigma$  significance.

ure 2 with respective identifying indices. Some of these counter-images will likely be confirmed with the forthcoming ACS observations of Abell 2744 which will provide deeper optical images allowing to tests of their multiplicity and thus corroborating the high redshift nature of these candidates (e.g., Ellis et al. 2001; Kneib et al. 2004) as well as the robustness of our lens modeling procedure.

#### 4. THE UV LUMINOSITY FUNCTION AT $Z = 7 - 8$

We now turn to estimating the rest-frame UV luminosity function (LF) at redshift  $z \sim 6 - 7$  and  $8$  using the two galaxy samples assembled above. We first determine the absolute magnitude of each source in the  $J_{125}$  band at a mean redshift of  $z \sim 6 - 7$  and in the  $H_{140}$  filter at  $z \sim 8$ . The observed values need to be corrected for the gravitational lensing magnification. While amplifying the intrinsic flux of a given source, strong lensing also distorts and stretches the source plane volume where it lies. The resultant drawback is that therefore a higher-magnification region will necessarily probe a smaller co-moving volume. Therefore, we need to account for these two effects in our LF estimates. The LF is given by

$$\phi(M)dM = \frac{N_i}{V_{eff}(M_i)} \quad (3)$$

where  $N_i$  is the number of galaxies in the  $i$ th bin and  $V_{eff}$  is the associated effective survey volume. Our effective volume is also determined by the shape of the redshift selection function, which is computed by simulating our selection procedure with artificial source galaxies. We generated starburst templates from Kinney et al. (1996) library, which were shifted to the desired redshifts, then we applied attenuation of  $A_V = 0-1$ , and calculated synthetic fluxes using filter throughputs before applying our selection criteria 1 and 2. Finally, we incorporate incompleteness correction in the selection function by performing our selection procedure on simulated galaxies. This is done by creating artificial galaxies using ARTDATA package in IRAF, exploring the parameter space of observed magnitudes, colors and position in the image. We assume a gaussian profile for the galaxy shape and add the simulated galaxies to the actual optical and IR images. We then apply our source extraction and color-color selection on the new images. Given our stringent selection criteria, the incompleteness function is dominated by the contamination of the photometry by bright sources in the crowded field.

The effective survey volume for each magnitude bin is calculated according to the following equation

$$V_{eff} = \int_0^\infty \int_{\Omega > \Omega_{min}} \frac{dV_{com}}{dz} f(z, m, \mu) d\Omega(\mu, z) dz \quad (4)$$

where  $\Omega_{min}$  is the source plane area with a minimum magnification  $\mu_{min}$  required to detect a galaxy with an apparent magnitude  $m$ .  $f(z, m, \mu)$  is the completeness function including the redshift selection function, and  $d\Omega(\mu)$  is the area element in the source plane as a function of the magnification factor.

The results are shown in Fig. 5 where our luminosity distribution is compared with previous results at  $z \sim 6$

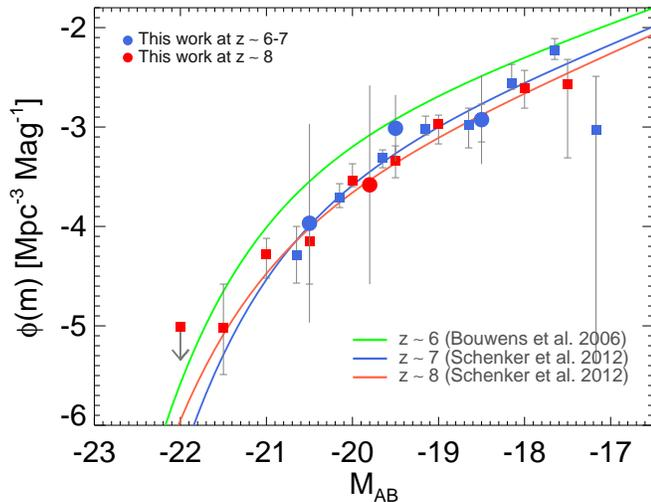


FIG. 5.— Rest-frame UV luminosity function at  $z \sim 6-8$  based on our  $I_{814}$  and Y105 dropout samples. The blue circles represent our LF determination at  $z \sim 6-7$  compared to previous results in the blank fields at  $z \sim 6$  (green line, Bouwens et al. 2006) and  $z \sim 7$  (blue squares and blue line, Schenker et al. 2012). The red circle is the estimate at  $z \sim 8$  compared to the HUDF12 determination at the same redshift (red squares and red line, Schenker et al. 2012). Error bars correspond to  $1-\sigma$  uncertainties.

to 8. At redshifts  $z = 6-7$  we use three bins in magnitude (-18.5, -19.5, -20.5), whereas we only have one candidate at  $z \sim 8$ . Overall, our derived LF is in good agreement with blank field results from the Hubble Ultra Deep Field (HUDF, Bouwens et al. 2006) and HUDF12 (Schenker et al. 2012). The uncertainties on the LF determination are dominated by poisson errors due to the small number statistics and to a lesser extent by cosmic variance.

## 5. CONCLUSION

The first HFF result we report here is important in regards to unraveling the properties and distribution of high-redshift galaxies since it confirms previous survey results derived from completely independent fields and therefore unequivocally demonstrates the feasibility of surveys using gravitational lensing fields. The agreement with previous blank field determinations of the LF also points to the robustness of our mass models and hence our modeling procedure. Despite the current limited depth of the observations (soon to be rectified once the HFF/ACS observations are completed), our LF reaches down to an intrinsic magnitude of  $M_{abs} \sim -18.5$  at  $z \sim 6-7$ , which corresponds to about  $0.2L_{z=7}^*$ , bolstering the advantage gained from gravitational magnification.

With the completed observations of the proposed six lensing clusters, the HFF program will probe the high-redshift Universe to unprecedented depths. For the same exposure time, HFF observations of A2744 will sample the faint-end of the LF 1.2 mag deeper than typical blank field (such as the UDF) with the aid and enhancement provided by these “cosmic telescopes”. We have shown here the feasibility and the effectiveness of such studies and the robustness of our cluster mass models, which will gain even more accuracy as new candidates and ever more multiply-imaged systems are discovered, identified and confirmed. The LF of these highest redshift galaxies is a key signature and determinant of the sources responsible for re-ionization of the Universe. Unmasking these sources with the help of the additional magnifying power offered by cluster-lenses looks not only promising but also very feasible as seen in these first results presented here.

HA and JPK are supported by the European Research Council (ERC) advanced grant “Light on the Dark” (LIDA). PN acknowledges support from NSF theory grant AST-1044455 and a theory grant from Space Telescope Science Institute hst-ar1214401.A. ML acknowledges support from CNRS. NL is supported by the Spanish Ministerio de Ciencia e Innovacion, under projects AYA2010-21766-C03-01 and AYA2010-21697-C05-0.

## REFERENCES

- Alavi, A., et al. 2013, ArXiv e-prints  
Atek, H., et al. 2011, *The Astrophysical Journal*, 743, 121  
Bertin, E., & Arnouts, S. 1996, *Astronomy and Astrophysics Supplement Series*, 117, 393  
Bolzoniella, M., Miralles, J.-M., & Pelló, R. 2000, *A&A*, 363, 476  
Bouwens, R. J., Illingworth, G. D., Blakeslee, J. P., & Franx, M. 2006, *ApJ*, 653, 53  
Bouwens, R. J., et al. 2009, *ApJ*, 690, 1764  
Bouwens, R. J., et al. 2012, *The Astrophysical Journal*, 754, 83  
Brammer, G. B., et al. 2012, *ApJ*, 758, L17  
Bruzual, G., & Charlot, S. 2003, *Monthly Notices of the Royal Astronomical Society*, 344, 1000  
Casertano, S., et al. 2000, *The Astronomical Journal*, 120, 2747  
Coleman, G. D., Wu, C.-C., & Weedman, D. W. 1980, *ApJS*, 43, 393  
Ellis, R., Santos, M. R., Kneib, J.-P., & Kuijken, K. 2001, *ApJ*, 560, L119  
Finkelstein, S. L., et al. 2013, *Nature*, 502, 524  
Giavalisco, M., et al. 2004, *The Astrophysical Journal*, 600, L103  
Hayes, M., Laporte, N., Pelló, R., Schaerer, D., & Le Borgne, J.-F. 2012, *Monthly Notices of the Royal Astronomical Society: Letters*, 425, L19  
Kashikawa, N., et al. 2006, *The Astrophysical Journal*, 648, 7  
Kinney, A. L., Calzetti, D., Bohlin, R. C., McQuade, K., Storchi-Bergmann, T., & Schmitt, H. R. 1996, *The Astrophysical Journal*, 467, 38  
Kneib, J.-P., Ellis, R. S., Santos, M. R., & Richard, J. 2004, *ApJ*, 607, 697  
Kneib, J.-P., & Natarajan, P. 2011, *A&A Rev.*, 19, 47  
Krist, J. E., Hook, R. N., & Stoehr, F. 2011, 20 years of Hubble Space Telescope optical modeling using Tiny Tim (SPIE - International Society for Optical Engineering), 81270J-81270J-16  
McLure, R. J., et al. 2011, *Monthly Notices of the Royal Astronomical Society*, 418, 2074  
Merten, J., et al. 2011, *Monthly Notices of the Royal Astronomical Society*, 417, 333  
Oesch, P. A., et al. 2010, *The Astrophysical Journal*, 709, L16  
Ono, Y., et al. 2012, *ApJ*, 744, 83  
Ouchi, M., et al. 2010, *The Astrophysical Journal*, 723, 869  
Richard, J., Kneib, J.-P., Ebeling, H., Stark, D. P., Egami, E., & Fiedler, A. K. 2011, *Monthly Notices of the Royal Astronomical Society: Letters*, 414, L31  
Salpeter, E. E. 1955, *The Astrophysical Journal*, 121, 161

TABLE 2  
PHOTOMETRIC AND COLOR MEASUREMENTS FOR THE  $z \sim 6 - 7$  DROPOUTS

Target	R.A. (J2000)	Dec (J2000)	$I_{814} - Y_{105}$	$Y_{105} - J_{125}$	$J_{125}$	Magnification <sup>a</sup>	Photo- $z$
93	3.593807	-30.415442	> 1.34	-0.03 ± 0.02	26.49 ± 0.01	3.42 ± 0.19	6.8
171	3.570648	-30.414662	1.89 ± 0.31	0.08 ± 0.02	26.59 ± 0.02	1.57 ± 0.03	6.3
561	3.603225	-30.410330	> 0.8	-0.10 ± 0.03	27.37 ± 0.03	3.75 ± 0.19	7.5
632	3.593541	-30.409719	1.46 ± 0.16	-0.06 ± 0.02	26.71 ± 0.02	6.28 ± 0.56	5.9
841	3.606378	-30.407279	2.18 ± 0.31	-0.01 ± 0.03	26.96 ± 0.02	2.27 ± 0.07	6.4
1127	3.580442	-30.405039	1.89 ± 0.36	0.09 ± 0.03	27.07 ± 0.02	4.71 ± 0.36	6.4
1180	3.600068	-30.404382	1.47 ± 0.26	-0.23 ± 0.04	27.69 ± 0.03	4.81 ± 0.40	6.2
1192	3.576128	-30.404494	1.23 ± 0.10	0.06 ± 0.01	26.33 ± 0.01	2.92 ± 0.14	6.1
1265	3.570062	-30.403720	> 0.8	0.15 ± 0.02	26.88 ± 0.02	1.95 ± 0.05	7.0
1266	3.601099	-30.403956	2.09 ± 0.47	0.19 ± 0.03	26.99 ± 0.02	3.51 ± 0.22	6.5
1521	3.600541	-30.401804	1.12 ± 0.22	-0.03 ± 0.04	27.48 ± 0.03	3.04 ± 0.16	5.9
2276	3.606503	-30.380974	> 0.8	0.79 ± 0.07	26.47 ± 0.02	1.38 ± 0.02	7.4
2715	3.596100	-30.385832	> 0.8	0.74 ± 0.05	26.97 ± 0.02	2.06 ± 0.07	5.9
2770	3.606230	-30.386646	1.32 ± 0.15	0.16 ± 0.02	26.51 ± 0.02	1.52 ± 0.03	5.5
3284	3.576655	-30.391364	2.56 ± 0.07	0.22 ± 0.00	24.18 ± 0.00	5.82 ± 0.55	6.5
3458	3.603540	-30.393106	0.91 ± 0.10	0.03 ± 0.02	26.75 ± 0.02	1.77 ± 0.05	6.0
3761	3.597850	-30.395970	> 0.77	0.36 ± 0.03	27.21 ± 0.03	2.79 ± 0.13	6.7
Target	R.A. (J2000)	Dec (J2000)	$Y_{105} - J_{125}$	$J_{125} - H_{140}$	$H_{140}$		
2070	3.604522	-30.380463	1.07 ± 0.03	0.30 ± 0.02	26.23 ± 0.01	1.47 ± 0.02	8.35

<sup>a</sup>this is the flux amplification factor

TABLE 3  
MULTIPLE-IMAGE SYSTEMS AT  $z \sim 6 - 8$

Image	Target	R.A. (J2000)	Dec (J2000)	$I_{814} - Y_{105}$	$Y_{105} - J_{125}$	$J_{125}$
1.1	1192	3.576128	-30.404494	1.23 ± 0.10	0.06 ± 0.01	26.33 ± 0.01
1.2	3822	3.591436	-30.396687	1.66 ± 0.22	-0.07 ± 0.03	27.32 ± 0.02
2.1	1291	3.584396	-30.403395	1.12 ± 0.17	-0.05 ± 0.03	27.63 ± 0.03
2.2	1291b	3.584741	-30.403147	...	...	> 27.8
3.1	632	3.593541	-30.409719	1.46 ± 0.16	-0.06 ± 0.02	26.71 ± 0.02
3.2	1521	3.600541	-30.401804	1.12 ± 0.22	-0.03 ± 0.04	27.48 ± 0.03
4.1	410	3.585800	-30.411740	1.04 ± 0.15	-0.03 ± 0.02	27.06 ± 0.02
4.2	1180	3.600068	-30.404382	1.47 ± 0.26	0.23 ± 0.04	27.69 ± 0.03
4.3	673	3.596525	-30.409031	1.69 ± 0.43	0.33 ± 0.07	27.41 ± 0.03
5.1	1127	3.580442	-30.405039	1.89 ± 0.36	0.09 ± 0.03	27.07 ± 0.02
5.2	1956	3.585321	-30.397960	> 0.36	0.09 ± 0.03	27.35 ± 0.02
5.3	3761	3.597850	-30.395970	> 0.23	0.36 ± 0.04	26.21 ± 0.03
5.4	1327	3.587268	-30.403279	> 0.18	0.12 ± 0.04	27.50 ± 0.03

Schenker, M. A., Stark, D. P., Ellis, R. S., Robertson, B. E.,  
Dunlop, J. S., McLure, R. J., Kneib, J.-P., & Richard, J. 2012,  
ApJ, 744, 179

Stark, D. P., Ellis, R. S., Chiu, K., Ouchi, M., & Bunker, A. 2010,  
MNRAS, 408, 1628  
Steidel, C. C., Giavalisco, M., Pettini, M., Dickinson, M., &  
Adelberger, K. L. 1996, The Astrophysical Journal, 462, L17  
Vanzella, E., et al. 2011, ApJ, 730, L35